

NOVEL PRECISION ENHANCEMENT ALGORITHM WITH REDUCED IMAGE NOISE IN COSMIC MUON TOMOGRAPHY APPLICATIONS

by

Sangkyu LEE, Amanda FOLEY, and Tatjana JEVREMOVIC *

The Utah Nuclear Engineering Program, University of Utah, Salt Lake City, USA

Scientific paper
DOI: 10.2298/NTRP1601051L

In this paper, we present a new algorithm that improves muon-based generated tomography images with increased precision and reduced image noise applicable to the detection of nuclear materials. Cosmic muon tomography is an interrogation-based imaging technique that, over the last decade, has been frequently employed for the detection of high- Z materials. This technique exploits a magnitude of cosmic muon scattering angles in order to construct an image. The scattering angles of the muons striking the geometry of interest are non-uniform, as cosmic muons vary in energy. The randomness of the scattering angles leads to significant noise in the muon tomography image. GEANT4 is used to numerically create data on the momenta and positions of scattered muons in a predefined geometry that includes high- Z materials. The numerically generated information is then processed with the point of closest approach reconstruction method to construct a muon tomography image; statistical filters are then developed to refine the point of closest approach reconstructed images. The filtered images exhibit reduced noise and enhanced precision when attempting to identify the presence of high- Z materials. The average precision from the point of closest approach reconstruction method is 13 %; for the integrated method, 88 %. The filtered image, therefore, results in a seven-fold improvement in precision compared to the point of closest approach reconstructed image.

Key words: muon tomography, multiple Coulomb scattering, GEANT4, nuclear material

INTRODUCTION

Cosmic muon tomography is theoretically founded on the principle of multiple Coulomb scattering (MCS) [1]. The interaction of cosmic ray muons with matter is mainly through a Coulomb interaction between electrons and atomic nuclei. Interactions with electrons lead to continuous energy loss and muon stopping via ionization; interactions with nuclei result in angular diffusion [2]. This angular diffusion provides the basis for applications of cosmic ray muon tomography in cargo container scanning. In general, the theory of MCS predicts a scattering angular distribution for the Coulomb interactions between charged particles and atoms [3]. Lynch [4] extended Moliere's theory¹ to heavy charged particles such as muons, and derived a general formula for the MCS of muon particles. According to this MCS formula, muon scattering angles are determined by material properties that pre-

dominantly depend on the atomic number and density of the penetrating materials. Due to its dependency on atomic number and density, cosmic muon tomography has been studied for the detection of concealed high- Z materials [1]. In addition to Coulomb interactions, the flux and energy of cosmic muons provide the means for tomography to be applicable for large-scale interrogation imaging. The flux of cosmic muons at sea level is equal to 1 muon/cm²/min, while the energy of the cosmic muons ranges from 0.1 GeV to 100 GeV [5]. The energy of cosmic muons is high enough for Coulomb scattering to be observed when muons pass through high- Z materials [6]. However, cosmic muons do not have uniform scattering angle distributions when interacting with certain materials, due to their varied energies [5]. This leads to significant noise production in the tomography image. In order to reduce this noise, filtering techniques must be used. Previous studies

* Corresponding author; e-mail: tatjana@chemeng.utah.edu

¹ Moliere's theory explains multiple Coulomb scattering of electrons and other charged particles

have explored the application of such filters. A statistical filtering method is used to reduce noise, with the filtered output resulting in a well-refined image [7]. Another study applied the median filter and the Gaussian filter independently to reduce noise [8]. This application efficiently removed noise in the muon tomography image.

This paper introduces a novel method based on the use of synthesized statistical filtering methods to reduce noise and improve the precision of muon-based tomography. This method is developed using muon tomography images created using GEANT4. Numerically derived muon momenta and positions are then reconstructed in order to create a tomography image using the point of closest approach (PoCA) reconstruction technique. An integrated filtering algorithm is then compared to the median, mean and Gaussian filtering methods, providing good agreements.

MUON CHARACTERISTICS, TOMOGRAPHY AND INTERACTIONS

Muon characteristics

The muon (μ) is an elementary particle similar to the electron, with an electric charge of $(-1e)$ and $1/2$ spin, but with a much greater mass than an electron. Table 1 shows the relationship between the muon and other subatomic particles. The muon is a type of Lepton, meaning it does not have any further sub-structure. It is unstable due to its mean lifetime² of $2.2 \mu\text{s}$. Similar to other elementary particles, the muon has a corresponding antiparticle, the antimuon; the antimuon has opposite charge $(+1e)$ and equal mass and spin as the muon. Muons are denoted in this paper by μ^- , and antimuons by μ^+ .

Muons were discovered by Carl D. Anderson and Seth Neddermeyer in 1936, while measuring the energy loss of particles occurring in cosmic ray show-

Table 1. Characteristics of elementary particles in Fermions and Bosons groups: muon is located in the group of Fermions within the Lepton category [9]

	Fermions (three families of matter)			Bosons (force carriers)
	I	II	III	
Quarks	u up	c charm	t top	γ photon
	d down	s strange	b bottom	Z Z boson
Leptons	ν_e electron neutrino	ν muon neutrino	ν tau neutrino	W W boson
	e electron	μ muon	τ tau	g gluon

² Mean lifetime is inversely proportional to the decay constant or it is equal to half-life multiplied with $\ln 2$

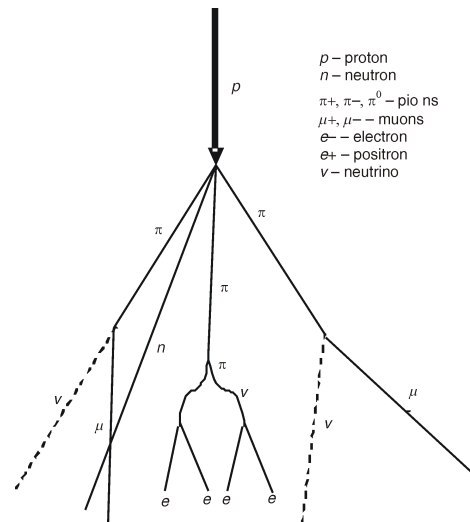


Figure 1. Cosmic ray air shower in the upper earth atmosphere. Cosmic ray proton enters the atmosphere creating a hadronic shower [13]

ers [10]. Anderson noticed that muon particles curved differently than electrons and other known particles when passing through a magnetic field. The projectile motion of the muon had a less sharp curve than that of an electron, due to its heavier mass of $105.7 \text{ MeV}/c^2$ compared to the mass $0.511 \text{ MeV}/c^2$ of an electron. This makes muons almost 200 times more massive than electrons [11]. Cosmic muons reach sea level with a flux of $1 \text{ muon}/\text{cm}^2/\text{min}$ [5]. The Earth's atmosphere is constantly exposed to cosmic rays. Cosmic ray protons are accelerated in deep space from supernova remnants that then interact in Earth's atmosphere, creating so-called cosmic ray hadronic showers illustrated in fig. 1 [12]. These protons interact and create other secondary particles; the muon is included among these secondary particles.

Highly energetic cosmic ray protons interacting with Earth's atmosphere create secondary particles including delta resonances and residual nuclei [14]. Production of delta resonance by proton collision with air follows $p + N \rightarrow \Delta + N$, where p represents protons, N is the nuclei of elements in the atmosphere, and Δ is the delta resonance.

The delta resonance produces a group of delta particles, $\Delta^-(ddd)$, $\Delta^0(udd)$, $\Delta^+(uud)$, and $\Delta^{++}(uuu)$ [11]. Charged pions can be produced from the following decay modes of Δ^- and Δ^{++} with the mean lifetime of $(5.63 \pm 0.14) \cdot 10^{-24} \text{ s}$ [14]

$$\Delta^- \rightarrow n + \pi^-: \text{Production of pion } (\pi^-) \text{ and neutron } (n) \text{ by } \Delta^- \text{ decay}$$

$$\Delta^{++} \rightarrow p + \pi^+: \text{Production of pion } (\pi^+) \text{ and proton } (p) \text{ by } \Delta^{++} \text{ decay}$$

These pions then decay with a mean lifetime of 26 ns , resulting in the production of a muon and a neutrino, or gamma rays, depending on the parent pion charge, as follows [11]

$\mu^- + \bar{\nu}_\mu$: Production of muon (μ^-) and anti-muon neutrino ($\bar{\nu}_\mu$) by π^- decay

$\mu^- \rightarrow \nu_\mu$: Production of muon (μ^-) and muon neutrino (ν_μ) by π^- decay

$\gamma + \gamma$: Production of two gamma rays (γ) by π^0 decay

Upon reaching the Earth's surface, muons either continue to slow down through additional interactions or decay with a 2.2 μ s mean lifetime [15]. Cosmic ray muons decay into an electron (or positron) and two neutrinos as follows

$\mu^- \rightarrow e^- + \bar{\nu}_e + \nu_\mu$: Production of electron (e^-), anti-electron neutrino ($\bar{\nu}_e$), and muon neutrino (ν_μ) by beta-decay of μ^-

$\mu^+ \rightarrow e^+ + \nu_e + \bar{\nu}_\mu$: Production of positron (e^+), electron neutrino (ν_e), and anti-muon neutrino ($\bar{\nu}_\mu$) by beta-decay of μ^+

Most cosmic ray muons are created near an altitude of 15 km above sea level [5]. As they pass through Earth's atmosphere, the cosmic ray muons typically lose about 2 GeV due to ionization. The average energy of a cosmic ray muon at the Earth's surface is 4 GeV. It seems that the 2.2 μ s mean lifetime is too short for a muon to travel 15 km from the atmosphere to sea level; however, the relativistic effect of a 4 GeV muon allows the muon to travel about 27 km during its mean lifetime, which is long enough to reach the surface of Earth.

Muon tomography

Tomography is defined as imaging by sections that may be visualized in three dimensions. One of the first applications of tomography used X-rays to generate images of areas inside of the human body; the X-ray source and film were moved in different directions to produce sectional images [16]. Medical imaging still relies on tomography for techniques such as positron emission tomography (PET), single photon emission computed tomography (SPECT), and computed tomography (CT) scans [17]. Cosmic muon tomography is applied to various fields, such as geological mapping, nuclear reactor imaging, and cargo scanning. Muon tomography has also been proposed as a method for volcanic activity prediction; this application is based in the measurement of cosmic muon flux scattering in geological structures [18]. In nuclear reactor analysis, muon tomography is adopted to identify the location and status of nuclear fuels. A muon imaging system developed at Los Alamos National Laboratory will be deployed at the Fukushima Daiichi power plant in Japan by the end of 2015 [19]. Cosmic muons have also been applied to cargo scanning, with the intent to detect shielding materials and special nu-

clear materials (SNM) [1]. The muon flux reaching Earth's surface is enough to be applied in the tomography of large volumes such as reactors or cargo containers. This means that muon tomography does not require an artificial source. The principle of muon tomography exploits the multiple Coulomb scattering; the scattered angular width determines the material properties [1].

Muon tomography requires two sets of detectors that sandwich the examined volume; these detectors provide information about muon scattering angles, indicating the presence of certain materials in the examined volume. These data are analyzed with the algorithms in order to construct a 3-D image. One typical reconstruction method is the PoCA [20]. The PoCA method finds the closest point between two linear muon tracks and estimates a final scattering angle between them. The PoCA method is discussed in detail in the section *Point of closest approach to reconstruct muon tomography images*.

Muon interactions and multiple muon coulomb scattering

To accurately explore the use of muon tomography, an understanding of muon interactions and multiple Coulomb scattering is needed. Those muon interactions of interest include ionization, bremsstrahlung, pair production and muon-nucleus inelastic scattering. The energy loss due to these interactions is generally expressed as follows [21]

$$\frac{dE}{dx} = \frac{dE}{dx}_i + \frac{dE}{dx}_b + \frac{dE}{dx}_p + \frac{dE}{dx}_n \quad (1)$$

where „i” denotes ionization, „b” denotes bremsstrahlung, „p” denotes pair production, and „n” denotes nucleus inelastic scattering. These interactions are responsible for any energy loss as the muon penetrates a material, and affect the angle deflection due to MCS [22]. Therefore, in this section, these four major muon interactions and MCS are described in a greater detail.

Ionization. Muons lose their energy by ionizing the matter they interact with; this is because no charged particles may avoid losing energy through the ionization of matter. The ionization process is responsible for a continuous loss of muon energy due to the interaction of the particle with atomic electrons in the material. The rate at which this energy loss occurs is well-described by the Bethe-Bloch formula [23]; for a given material, the differential energy loss function depends on the kinetic energy of a muon, as follows

$$\frac{dE}{dx} = 4\pi N_A m_e c^2 z^2 \frac{e^2}{4\pi\epsilon_0 m_e c^2} \frac{Z}{A} \frac{1}{\beta^2} \left[\frac{1}{2} \ln \frac{2m_e \beta^2 \gamma^2 T_{\max}}{I^2} - \beta^2 \frac{\delta(\beta\gamma)}{2} \right] \quad (2)$$

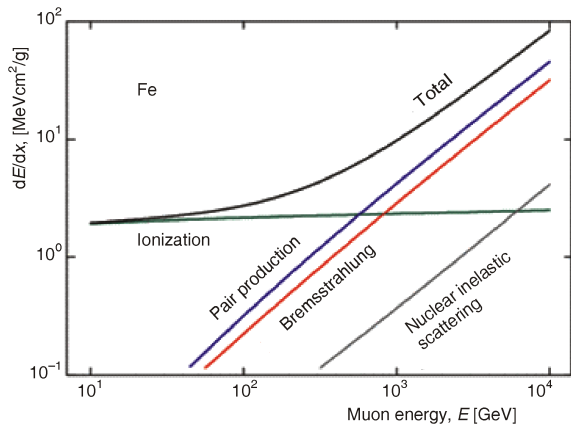


Figure 2. Energy loss of muons interacting with iron [24]. Muon energy loss is determined by the incident muon energy as well as its interactions (ionization, bremsstrahlung, pair production, and nuclear inelastic scattering)

where dE/dx , or stopping power, is the change in kinetic energy E over a distance x , N_A – the Avogadro's number, $m_e c^2$ – the electron rest mass energy, z – the unit charge of the incident muon, $(e^2/4\pi\epsilon_0 m_e c^2)$ is a classical electron radius, Z – the atomic number, A – the atomic mass, γ – the Lorentz factor³, I – the mean excitation energy of the ionized atom, in eV, T_{\max} – the incident muon energy, and $\delta(\beta\gamma)$ represents a density effect correction to ionization energy loss. As an example to illustrate muon energy loss, fig. 2 shows the trend in energy loss of a muon interacting with iron. In the energy region of less than a few hundred GeV, the ionization interaction dominates over other types of interactions. At high energies, over a thousand GeV, bremsstrahlung and pair production interactions dominate [24]. This is correlated to the cross section and wavelength of the muon; muons with longer wavelengths have greater probability of collision with electrons in a given material. The contribution of nuclear inelastic scattering interactions to the combined cross section is small compared to the contribution of all other interactions. However, nuclear inelastic scattering leads to the production of nuclear-electromagnetic showers, and it determines the main source of hadron background arising from high energy muon interactions [24].

Bremsstrahlung. Bremsstrahlung is electromagnetic radiation produced by the deceleration of a charged particle when deflected by another charged particle [25]. Muons produce bremsstrahlung while passing through the electric field of a nucleus. The muon bremsstrahlung cross section was originally calculated by Bethe [26]. The differential bremsstrahlung cross section for muon interaction with a nucleus field is defined as follows [27]

$$\left. \frac{d\sigma}{dv} \right|_{\text{brems, nucl}} \propto 2Z \frac{m_e}{M_\mu} r_e^2 \frac{4}{3} \frac{4}{3} v^2 \frac{3}{2} k \frac{M_\mu}{m_e} Z^{2/3} \frac{dv}{v} \ln \frac{k\sqrt{e} M_\mu^2 v}{2 m_e E_{\text{ou}} v} Z^{1/3} \quad (3)$$

where v is the fraction of the muon energy transferred to a photon, M_μ – the mass of the muon, r_e – the classical electron radius, k – a constant equal to 190, e represents natural logarithm of 2.718, and E_{ou} is initial energy of the muon. Equation (3) shows that the cross section for muon bremsstrahlung with a nucleus increases with atomic number; therefore, the number of photons emitted increases with the Z of a material. Muons may also interact with electrons as bremsstrahlung is produced. The cross section accounts for bremsstrahlung loss in interactions with atomic electrons. For that, the influence of the electron recoil is ignored, since it is negligible. Therefore, a much better approximation, which takes electronic binding into account, is given by [27]

$$\left. \frac{d\sigma}{dv} \right|_{\text{brems, nucl}} \propto 2Z \frac{m_e}{M_\mu} r_e^2 \frac{4}{3} \frac{4}{3} v^2 \frac{dv}{v} \ln \frac{2E_{\text{ou}}(1-v)}{M_\mu v} \quad (4)$$

The cross section for bremsstrahlung is a function of fractional energy transfer “ v ” as shown in eq. (4). Due to dependence on the fraction of the muon's energy transferred to a photon, the cross section increases with the high fractional energy transfer.

Direct Electron Pair Production. Direct electron pair production is one of the most important muon interactions. It involves the formation or materialization of two electrons, one electron and one positron, from the kinetic energy of the muon, usually in the vicinity of an atomic nucleus [14]. The cross section for direct electron pair production in a Coulomb field was first calculated by Racah [13].

Nuclear screening was later taken into account by Kelner and Kotov [28]. With their approach, the average energy loss is obtained through a numerical integration, as follows

$$b_{\text{pair, nucl}} = \frac{1}{E} \left. \frac{dE}{dx} \right|_{\text{pair, nucl}} = \frac{N_A}{A} \int_0^1 v \frac{d\sigma}{dv} dv \quad (5)$$

where $d\sigma/dv$ is the differential cross section for pair production. This equation is widely used in muon transport calculations. The pair production due to interactions with atomic electrons is defined as follows [13]

³Lorentz factor connects time, length, and relativistic mass change for a moving particle

$$b_{\text{pair, nucl}} [\text{cm}^2 \text{g}^{-1}] = \frac{1}{E} \frac{dE}{dx} \Big|_{\text{pair, elec}}$$

$$\frac{Z}{A} 0.073 \ln \frac{2E}{M_\mu} \frac{1}{1 - \frac{gZ^{2/3}E}{M_\mu}} 0.31 \cdot 10^{-6} \quad (6)$$

where $g=4.4 \cdot 10^{-5}$ is defined for hydrogen and $g=1.95 \cdot 10^{-5}$ refers to other materials. These constants including g are obtained from numerical analysis [13]. It can be seen, according to eq. (5) and eq. (6), that the energy loss from pair production decreases by increasing the atomic mass, A , of the interacting atoms.

Nuclear inelastic interactions. At high muon energies, the inelastic interaction of muons with nuclei is the dominant interaction type. In this energy region, many simplifications can be made in order to obtain convenient and simple relations for the interaction cross section. For inclusive scattering where the scattering amplitudes are summed over all possible hadronic final states, the unpolarized cross section can be written as a function of two independent kinematic variables [29]. Therefore, the differential cross section for unpolarized deep-inelastic charged lepton scattering can be written, in the Born approximation, as [30]

$$\frac{d^2\sigma}{dQ^2 dx} = \frac{4\pi\alpha^2}{Q^4} \frac{1}{x} xy^2 F_1(x, Q^2) + y \frac{Mxy}{2E} F_2(x, Q^2) \quad (7)$$

where α is the electromagnetic coupling constant and $F_1(x, Q^2)$ and $F_2(x, Q^2)$ are the unpolarized structure functions of the nucleon.

$$Q^2 = -q^2 = -(k - k')^2 = 4EE' \sin^2\theta$$

is the squared four-momentum transfer. In this equation, k, k', p and q are the four-vectors of the initial and final state lepton, the target nucleon, and the exchanged boson. $v = pq \cdot M = E' - E$ is the energy transferred to the hadronic system. M is the mass of the target nucleon, whereas the lepton mass has been neglected. E, E' , and θ are the energies of the incident and scattered lepton, and the lepton scattering angle, in the laboratory frame. Here, $x = Q^2/2pq = Q^2/2Mv$ and $y = pq/pk = v/E$ are the scaling variables.

Multiple muon coulomb elastic scattering. The interaction of a muon with a nucleus results in its angular deflection [13]. This angular deflection provides the basis for applications of cosmic ray muons in tomography [1]. When a muon passes through matter, it is deflected by a certain scattering angle. These deflections are due to Coulomb interactions between muons and atoms, since muons are charged particles [5]. Cosmic muons that penetrate a given medium undergo MCS events due to their energetic nature. The theory of multiple Coulomb scattering was developed by Bethe [31]; in this method, the muon scattering angu-

lar distribution was assumed to follow a Gaussian distribution. The Gaussian function is defined as the probability density function (PDF) for a differential number of particles, which corresponds to the specific angle as follows [1]

$$\frac{dN}{d\theta_x} = \frac{1}{\sqrt{2\pi}\theta_0} e^{-\frac{\theta_x^2}{2\theta_0^2}} \quad (8)$$

where N is the number of muons, θ_x – the scattering angle in the 2-D plane, and θ_0 – the root mean square (RMS) of the scattering angle distribution. Along with the 2-D Gaussian distribution, tomography considers a 3-D image. Therefore, the spatial angle, θ^{space} , is defined as the scattering angle between the incident and scattered muons in 3-D space. The projection of a scattered angle onto the 2-D plane is defined with $\theta^{\text{plane,x}}$ in the y - z plane and with $\theta^{\text{plane,y}}$ in the x - z plane. The RMS width for each angular distribution is $\theta_0, \theta_{\text{RMS}}^{\text{plane,x}}, \theta_{\text{RMS}}^{\text{plane,y}}$, because, according to the MCS, θ is defined as an RMS width of scattered angles projected on the planes [32]. An RMS width in the y - z plane, $\theta_{\text{RMS}}^{\text{plane,x}}$, and an RMS width in the x - z plane, $\theta_{\text{RMS}}^{\text{plane,y}}$, are orthogonal to the z direction, so it can be derived as follows

$$(\theta_{\text{RMS}}^{\text{space}})^2 = (\theta_{\text{RMS}}^{\text{plane,x}})^2 + (\theta_{\text{RMS}}^{\text{plane,y}})^2 \quad (9)$$

From there we obtain $\theta_0 = \theta_{\text{RMS}}^{\text{space}} / \sqrt{2}$ [33].

Based on the Gaussian function, the MCS is derived to estimate the root mean square (RMS) width of an angular distribution. The distribution can be estimated as a zero mean Gaussian for the central 98 % of the angles [4]. The MCS formula for muons is:

$$\theta_0 = \frac{13.6 \text{ MeV/c}}{p} \sqrt{\frac{x}{X_0}} \quad (10)$$

where 13.6 MeV/c is calculated by considering a distribution of the central 98 % of the angles, p [MeV/c] is the muon momentum, θ_0 [radian] is RMS of a scattering angle width, x [cm] is the material thickness, and X_0 [cm] is the radiation length, which represents an average travelling distance in a given material [4] defined with

$$X_0 = \frac{A}{4\alpha N_A Z(Z-1)r_e^2 \ln(183Z^{1.3})} [\text{gcm}^{-2}] \quad (11)$$

where Z and A are the atomic number and mass number of a material, respectively, and the constant of 183 represents an approximated parameterization of the Thomas-Fermi potential⁴ [34]. The simplified form of this equation is as follows [34]

$$X_0 = \frac{716.4}{\rho} \frac{A}{Z(Z-1)\ln(287/\sqrt{Z})} \quad (12)$$

where ρ (g/cm^3) is the density of interacting material.

⁴ The Thoms-Fermi potential is a theoretical approach to calculate the effects of electric field screening by electrons

Equations (10) and (12) introduce a correlation between the scattering angle and the atomic number, Z . The MCS sensitivity to Z provides an understanding of the discrimination between different materials of similar densities. The radiation length decreases with the charge density of a material. A high- Z material with high density has a shorter radiation length; therefore, muons will be deflected by a larger angle in a high- Z material [35]. For example, a 10 cm thick material will scatter a 3 GeV muon with an angle of 2.3 milliradians in water, 11 milliradians in iron and 20 milliradians in lead [1]. The scattering angle, therefore, increases with increasing- Z material. By tracking the scattering angles of individual muons, high- Z materials can be distinguished from low- or medium- Z materials. This principle is applied to cargo scanning to identify shielding materials, as described in the following sections.

STATISTICAL FILTERING METHODS AS APPLIED TO COSMIC MUON TOMOGRAPHY IMAGES

Point of closest approach to reconstruct muon tomography images

The magnitude of the muon scattering angle is determined by the interacting material density and atomic number as defined with eq. (10). In order to construct a tomography image from muon interactions, scattering angle and interaction positions are required. In this paper we present a reconstruction algorithm, developed to obtain scattering angles and interaction positions [36]. The Point of Closest Approach (PoCA) [20] is selected as a method for reconstructing the images. The PoCA reconstruction method is based on a geometrical method for finding a muon interaction point and a scattering angle between the incident and scattered muon. This method determines the closest point of two linear muon tracks to estimate a final scattering angle between them; this is illustrated in fig. 3.

The primary assumption in applying PoCA is that the MCS is neglected by assuming one scattering interaction between the initial and final muon tracks.

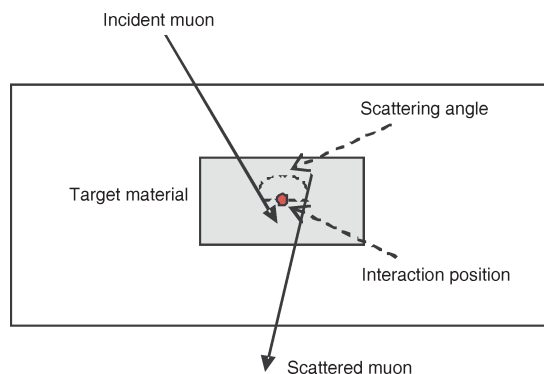


Figure 3. Illustration of the point of closest approach (PoCA)

Therefore, the angle between the incident vector and scattered vector is considered as the scattering angle, and the medium position of the point of closest approach is related to the position of interaction [37]. In the 2-D plane, if two lines are not parallel, they always intersect. However, the two lines may not intersect in 3-D space, even though they are not parallel. The PoCA reconstruction method may be used to find the closest point of the two vectors, in order to obtain the scattering interaction position, as follows

$$\vec{T}_1 \quad \vec{P}_1 \quad i\vec{V}_1 \quad \text{and} \quad \vec{T}_2 \quad \vec{P}_2 \quad i\vec{V}_2 \quad (13)$$

where \vec{T}_1 and \vec{T}_2 are the position vectors of the incident and scattered muon tracks, \vec{P}_1 and \vec{P}_2 are the initial and final position vectors, \vec{V}_1 and \vec{V}_2 are the momentum vectors, and i represents the i th position of the muon track. Hence, when \vec{T}_1 and \vec{T}_2 have the minimum distance of their i th positions, the middle point between those two positions is taken as the interaction position.

In a typical muon tomography system, gas electron multiplier (GEM) detectors detect the positions and directions of incident and scattered muons using a coincidence counting method [38]. In this paper, GEANT4 is used to generate these positions and directions for various muon energies and materials. GEANT4 is a toolkit used to simulate the transport of various subatomic particles, including muons, through matter [39]. The code includes muon cross-section data, and can therefore be used to track muon interactions. The GEANT4 model presented here consists of a 40 cm × 40 cm × 40 cm iron box with 0.5 cm thickness, as sketched in fig. 4. Inside this iron box, there are three 4 cm × 4 cm × 4 cm cubes of various materials, such as lead and uranium. Since it is a first validation test, we used a simple model to develop a preliminary image-filtering methodology. Other similar studies applied simplified geometries as well, such as 100 cm × 20 cm × 25 cm [35], 30 cm × 30 cm ×

30 cm [40], and 60 cm × 60 cm × 30 cm [41]. The GEANT4 model, sketched in fig. 4, includes four detectors used to record the muon tracks, providing information about the positions and momenta of both the incident and scattered muons. The two detectors at the top record the initial positions and vectors of the incident muons, while the two at the bottom record final positions and vectors of the scattered muons.

The GEANT4 simulated muon momenta are converted into muon scattering angles, θ^{space} , using the PoCA reconstruction approach based on the principle of arccosine [33], as follows

$$\theta^{\text{space}} = \arccos \frac{\vec{p} \cdot \vec{q}}{p \parallel q} \quad (14)$$

where \vec{p} is the vector of an incident muon, and \vec{q} is the vector of a scattered muon. This GEANT4 model is run with 100,000 histories to observe one hour of exposure time. The upper area is 1,600 cm² and the muon

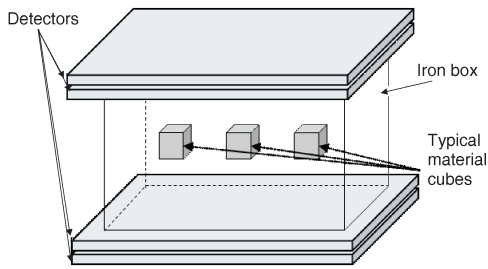


Figure 4. Geometric design for a GEANT4 model for generating muon tomography image

flux is counted at the rate of 1 muon/cm²/min at sea level [5]. The purpose of this model was to develop the filtering methodology; in this case, an exposure time of one hour is considered sufficient. Out of 100,000 muons, 2,400 muons scattered out of the geometry boundary; the remaining 97,600 muons provided the information required for the calculation of the interaction positions and scattering angles, based on eqs. (13) and (14), respectively. Figure 5 shows the PoCA reconstructed tomography image for the geometry illustrated in fig. 4. The high level of noise, produced as a result of varied cosmic muon energies, as described in the section *Muon characteristics*, is clearly observed in fig. 5. Various filtering methods are required to reduce this noise [7]. Here we present the statistical filtering methods of the median, the mean and the Gaussian smoothing techniques used to select the most efficient filtering method.

Statistical filtering methods

Median filtering: In signal processing, filtering reduces noise by emphasizing or suppressing structural signals in an image [42]. The median filter is a statistical filtering process used to reconstruct images; it is typically used to remove noise by finding a median value among selected pixels in 2-D or among voxels in

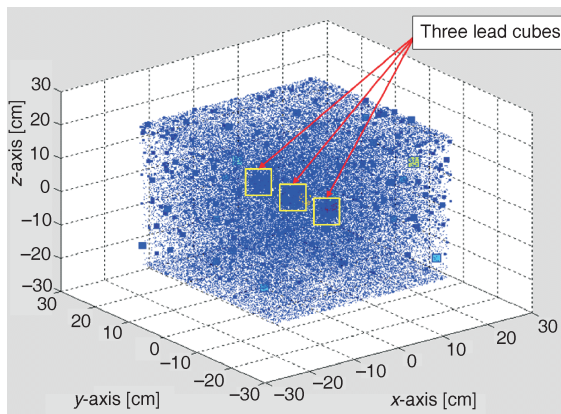


Figure 5. PoCA reconstructed muon tomography image generated with GEANT4 model of the cube shown in fig. 4 (in this figure three small cubes made of lead are placed inside a large iron hollow box)

5	8	2	→	7	7	7
7	6	9		7	7	7
12	7	4		7	7	7

Figure 6. Median filtering replaces each entry with the median value of the neighboring entries in a matrix, thus reducing the noise

3-D [42]. The median filter considers each pixel or voxel as a certain matrix, and it replaces the values of each pixel or voxel to the representative median value as illustrated in fig. 6.

For this filtering method, a voxel matrix is determined with each voxel size of 2 cm × 2 cm × 2 cm. Positions for each voxel are defined as follows

$$\text{Position } (p^{\text{th}} \text{ voxel}) \quad (l \ 1)NM \quad (m \ 1)N \quad n \quad (15)$$

where the *x*-axis has a grid numbering of 1, 2, ... *n* ... *N*; the *y*-axis is defined with the grid numbering of 1, 2, ... *m* ... *M*; and the *z*-axis is defined with the grid of 1, 2, ... *l* ... *L*.

Mean filtering. Mean filtering is another simple smoothing method used to reduce the noise in generated images. When noise varies randomly above and below a nominal brightness value, it can be reduced by averaging neighboring values [42].

The idea of mean filtering is simply to replace each pixel/voxel value with the average value of its neighbors, including its own value as shown in fig. 7. The original matrix has the same value as the one shown in fig. 6. It can be seen that the resulting mean filtering effect is different from the median filtering. The mean filtering method eliminates pixel/voxel values that are unrepresentative to their surroundings, such as salt and pepper noise. Therefore, the mean filtering method is generally used to produce a better estimate of the values, when the average is taken over a homogeneous area [43]. This mean filter is applied with the same size voxel of the median filter for the comparison to noise reduction. The average scattering angle in the *p*th voxel is defined as follows

5	8	2	→	6.7	6.7	6.7
7	6	9		6.7	6.7	6.7
12	7	4		6.7	6.7	6.7

Figure 7. Mean filtering replaces each entry with the mean value of the neighboring entries in a matrix thus reducing the noise

$$\text{Average scattering angle of } p^{\text{th}} \text{ voxel} = \frac{1}{N} \sum_{i=1}^N \text{scattering angle}_i \quad (16)$$

where N is total number of scattering angles in the p^{th} voxel.

Maxwell Boltzmann shift of mean values. According to Moliere's theory, the angular distribution of Coulomb scattered muons follows a Gaussian distribution. It is assumed that an average angle from the mean filter is the same as the mean of the Gaussian distribution [44]. However, the simulated scattering angle distributions show a statistical similarity with the Maxwell-Boltzmann distribution rather than with the Gaussian distribution.

Several cases are evaluated for muon multiple Coulomb scatterings, using 100,000 histories (or, one hour of exposure) in GEANT4; these cases are described in tab. 2. These cases are determined to observe muon scattering angles with low- Z (aluminum), medium- Z (iron), and high- Z (lead and uranium) materials for two different muon energies, 0.3 GeV for medium energy and 3 GeV for high energy. A solid box composed of aluminum, iron, lead or uranium is modeled for muon interactions. Figure 8 shows a GEANT4 model of muon scattering interactions with an aluminum, iron, lead or uranium box. Scattered angles of muons are calculated in 3-D space, using an inner product of arccosine given with eq. (14). Simulated scattering angle distributions are fitted with the Maxwell-Boltzmann distribution [45] based on eq. (17). For the ideal fitting, one additional parameter k is included in the general equation of the Maxwell-Boltzmann distribution, as follows

$$f(x) = \sqrt{\frac{2}{\pi}} \frac{\theta^{\text{space}2}}{a^3} \exp\left(-\frac{(\theta^{\text{space}} - k)^2}{2a^2}\right) \quad (17)$$

where θ^{space} is the spatial scattering angle, and a and k are coefficients of the distribution.

Table 2. Calculated root mean square (RMS) widths using eq. (10), as well as mode from eq. (18) and mean from eq. (19) for twelve scattering distributions

		Al	Fe	Pb	U
Thickness: 10 cm / Muon energy: 0.3 GeV	Mean	0.052	0.143	0.294	0.476
	Mode	0.047	0.132	0.265	0.422
	a	0.076	0.215	0.431	0.686
	k	0.202	0.571	1.143	1.809
	Chi-square	$1.19 \cdot 10^{-4}$	$4.85 \cdot 10^{-5}$	$3.22 \cdot 10^{-5}$	$2.98 \cdot 10^{-5}$
Thickness: 10 cm / Muon energy: 3 GeV	Mean	0.006	0.015	0.029	0.042
	Mode	0.005	0.013	0.027	0.038
	a	0.008	0.022	0.043	0.061
	k	0.022	0.057	0.115	0.163
	Chi-square	$2.58 \cdot 10^{-4}$	$5.72 \cdot 10^{-4}$	$2.10 \cdot 10^{-4}$	$1.35 \cdot 10^{-4}$
Thickness: 5 cm / Muon energy: 0.3 GeV	Mean	0.034	0.09	0.182	0.269
	Mode	0.031	0.081	0.162	0.239
	a	0.05	0.133	0.265	0.39
	k	0.134	0.353	0.704	1.035
	Chi-square	$2.04 \cdot 10^{-4}$	$7.36 \cdot 10^{-5}$	$4.27 \cdot 10^{-5}$	$3.86 \cdot 10^{-5}$

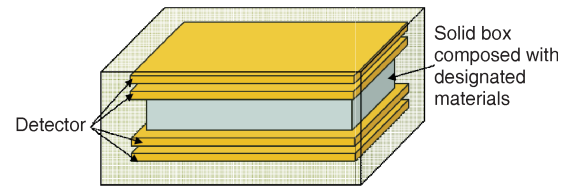


Figure 8. GEANT4 model of muon scattering interactions: The model utilizes an aluminum, iron, lead or uranium box (the thickness of each individual box is 5 cm or 10 cm as shown in tab. 2)

Figure 9 shows the fitting curves with the modified Maxwell-Boltzmann distribution, processed with the GEANT4 modeled scattering angle distributions. Figure 9 shows only one case, however the fitting processes are done for twelve cases of tab.2 to calculate the coefficients. In addition to these coefficients, the chi-square values estimated in tab. 2 are very small, indicating a well-fitting curve. The mode, which is the most frequently occurring value, has the same value with the mean in the Gaussian distribution due to the symmetrical shape of the plot; however, the mode is not equal to the mean in the Maxwell-Boltzmann distribution [46]. The mode of the modified Maxwell-Boltzmann distribution is as follows

$$\text{mode} = \frac{1}{2} (k + \sqrt{8a^2 - k^2}) \quad (18)$$

Table 2 introduces the calculated mode from eq. (18) and the mean from eq. (19) of each muon scattering distribution as shown in fig. 9. The mean of the discrete probability distribution is calculated using the following formula

$$\text{mean} = \frac{\sum_{i=1}^N x_i p(x_i)}{\sum_{i=1}^N p(x_i)} \quad (19)$$

where x_i denotes the numerically calculated muon scattering angles, and $p(x_i)$ is the probability of the scattering angle. These estimated means and modes are plotted in fig. 10, showing that they have a linear correlation.

The correlation of fig. 10 results in the following linear formula

$$\text{mode} = 0.88744 \text{ mean} + 0.00098 \quad (20)$$

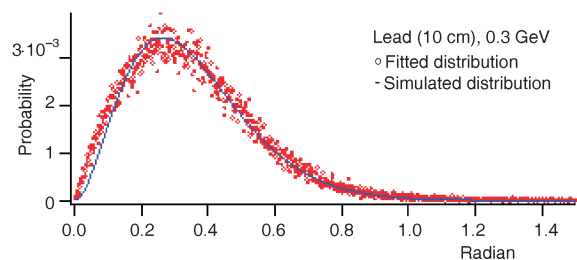


Figure 9. GEANT4 modeled muon scattering angle distribution and fitted Maxwell-Boltzmann distribution: Distributions are from modeling for lead (10 cm) with 0.3 GeV muon shown in tab. 2

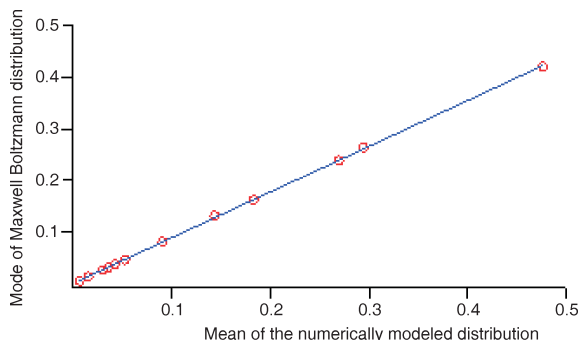


Figure 10. Mode of eq. (18) vs. mean of eq. (17): The mode and mean have a linear correlation to each value

Mean filtered tomography data are transferred into the Maxwell-Boltzmann shift defined with eq. (20), since it is assumed that the mode, which is the most frequently occurring angle, is the best value to represent the actual muon scattering angle. These shifted results are discussed in the section *Validation of the integrated statistical filtering method*.

Integrated filtering algorithm with Gaussian smoothing

The integrated filtering algorithm is developed to refine the PoCA reconstructed tomography image by fusing statics filtering methods. The algorithm follows three main steps: mean filtering, Maxwell Boltzmann shift, and Gaussian smoothing. Gaussian smoothing is similar to the mean filter; however, it reduces the weight of the input value with increasing distance from the center value, rather than weighing all input values equally from the mean filtering [42]. Gaussian smoothing effectively identifies concentrated points [47] and is suitable for finding dense points, such as high-Z materials, in a muon tomography image. This feature is used to create blurred images and remove noise by applying the following equation [47]

$$G_i(x, y) = \frac{1}{2\pi\sigma^2} e^{-\frac{x^2 + y^2}{2\pi\sigma^2}} \quad (21)$$

where σ is the standard deviation and x and y give the location on a plane. This formula may be applied only to the 2-D plane; tomography requires 3-D imaging. Therefore, eq. (21) is applied to generate refined images of x-y planes along the z-axis for the 3-D application. This Gaussian smoothing is used in the integrated filtering algorithm as shown in fig. 11. Mean filtered data is adopted as the first filtering step in the algorithm instead of median filtering, since the Maxwell-Boltzmann shift defined with eq. (20) exploits mean values to calculate the mode of the muon scattering angle distribution. After that, the Maxwell-Boltzmann shifted data is refined in the Gaussian smoothing filter using eq. (21). By analyzing the cumulative scattering angle ratio, the threshold of the scattering angle is set at 56 milliradians, which has

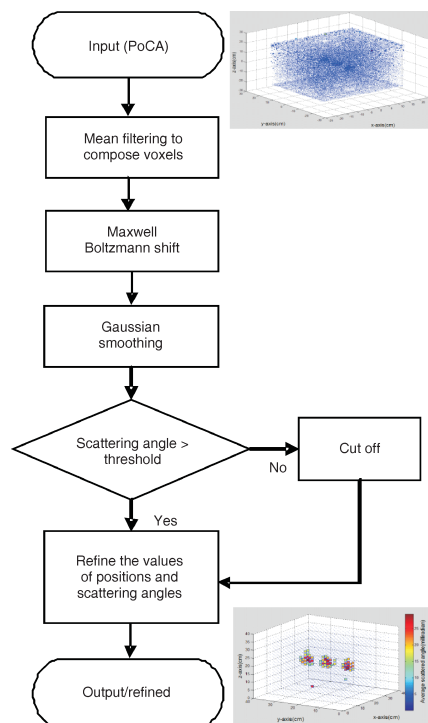


Figure 11. Schematics diagram of the integrated filtering method; this algorithm is applied to fully refine a GEANT4 generated muon tomography image

about a 95 % cumulative scattering angle ratio. Therefore, if a scattering angle is less than 56 milliradians, the angle is considered noise and the algorithm cuts off the values to refine the tomography image.

Thus, the following advantages can be expected by using the integrated filtering algorithm:

- The combined statistical filtering methods reduce random noise caused by cosmic muons.
- The algorithm decreases the uncertainty of estimated scattering angles to identify high-Z materials.
- The threshold of the scattering angle allows for the simulation to distinguish high-Z materials.
- The position identification method has the benefit of determining the location of interaction.

Despite the fact that the tomography images are filtered in the three steps of the mean filter, the Maxwell-Boltzmann shift, and the Gaussian smoothing, the integrated algorithm presented in fig. 11 requires a threshold to eliminate the noise scattering angles. The threshold is determined by modeling a scattering angle distribution of an empty box, which results in scattering interactions with only air. These simulated scattering angles are plotted in fig. 12.

VALIDATION OF THE INTEGRATED STATISTICAL FILTERING METHOD

Verification for noise reduction

The feasibility of the integrated filtering algorithm is tested by refining the simulated tomography

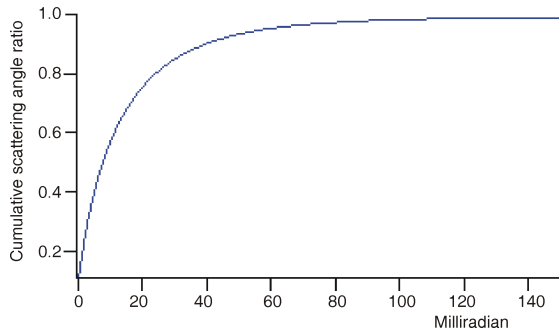


Figure 12. Cumulative scattering angle distribution of the MCS interaction with air: air (a low-density material) has that 95 % of the cumulative scattering angle is below 56 milliradians (based on the eqs. (10) and (12)); a saturation is thus for angles larger than 56 milliradians)

images. High-, medium- and low- Z materials were modeled to check the application for various conditions. The aim of this verification is to distinguish only high- Z and not medium- or low- Z materials. PoCA reconstructed images are used as input data for the filtering algorithm sketched in fig. 12. The voxel size for the statistical filtering methods is defined as $2\text{ cm} \times 2\text{ cm} \times 2\text{ cm}$. The reconstructed 3-D tomography images are compared to find the best performed filtering method. Figure 13 shows filtered images of three lead cubes inside a container, and the results show that the image from the integrated filtering algorithm is the best for noise reduction.

A standard deviation of 0.7 is selected for the Gaussian filtering method, as this value maximizes precision. The filtering results for tungsten and uranium cubes are shown in figs. 14 and 15, respectively. The true location of these three cubes is indicated with lined cubes in the plots.

Figures 13, 14, and 15 show the successful identification of high- Z materials. The filtering method is not expected to recognize medium- Z materials like iron or low- Z materials like aluminum; because of this, false identification of high- Z materials may be avoided. Figure 16 shows the filtered tomography images for aluminum and lead cubes inside containers, and it does not distinguish these materials. Although there is a small amount of random noise in fig. 16 (b), the integrated algorithm recognized no high- Z materials. The integrated algorithm is proven effective for noise reduction and the accurate discrimination of high- Z materials exclusively.

Precision improvement based on the integrated filtering algorithm

Verification of noise reduction using the integrated filtering algorithm is described in the section *Verification for noise reduction*; this verification, however, is not sufficient to confirm that the integrated filtering algorithm is the most effective one. For better evaluation in quantifying the detection performance

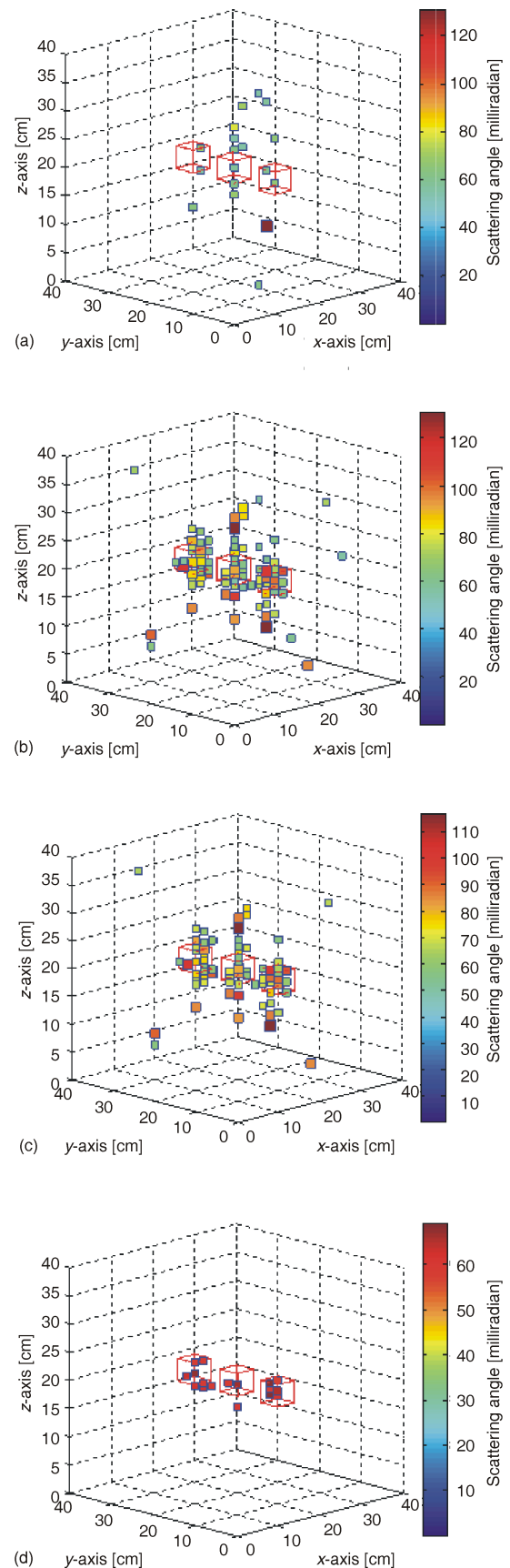


Figure 13. Refined cosmic muon tomography images of three lead cubes using (a) median filtering, (b) mean filtering, (c) mean filtering with Maxwell Boltzmann shift, and (d) integrated filtering algorithm

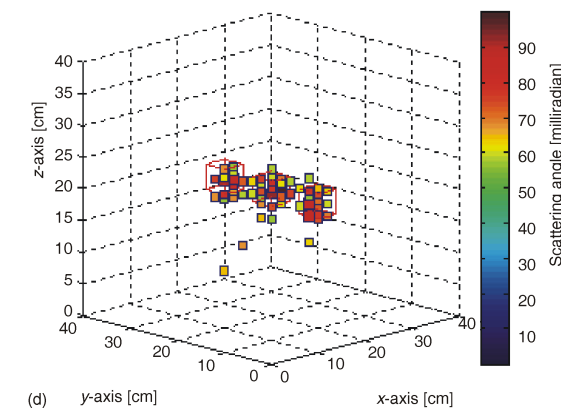
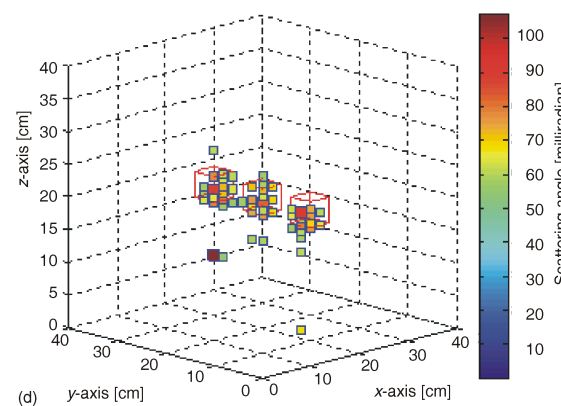
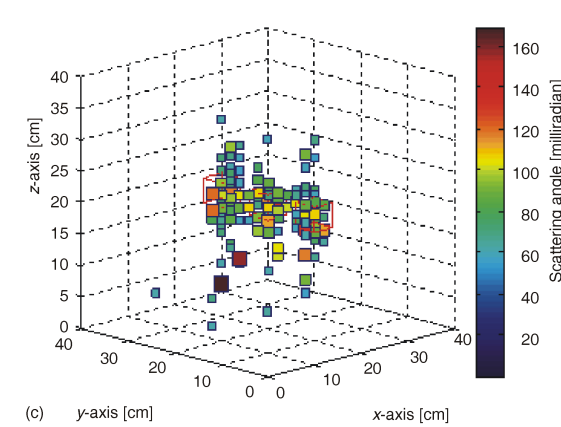
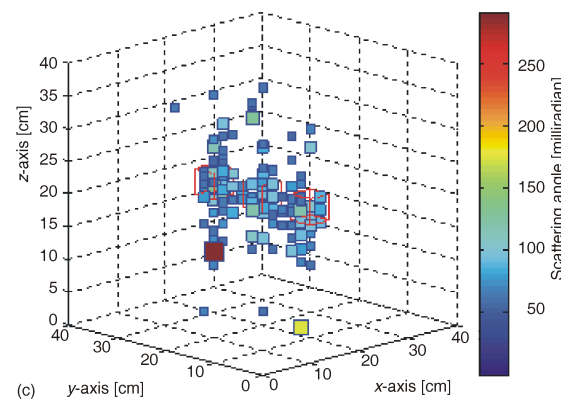
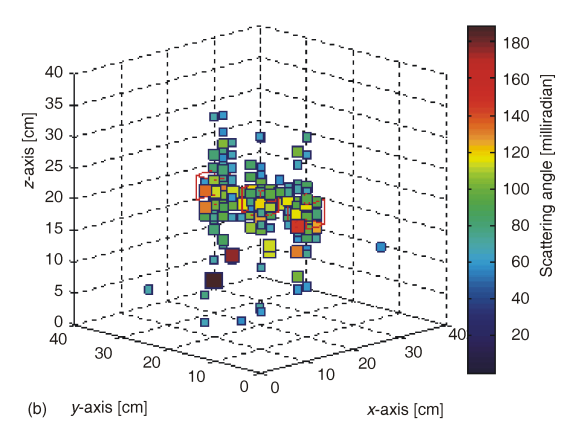
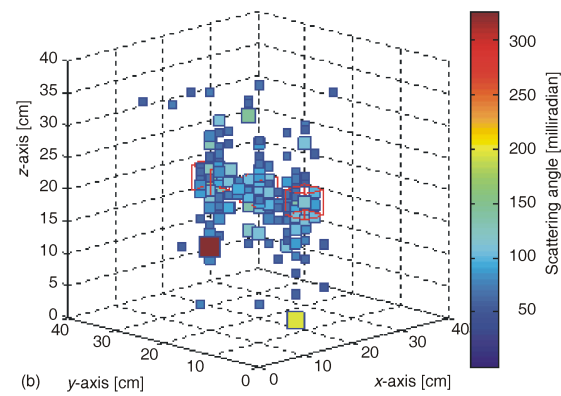
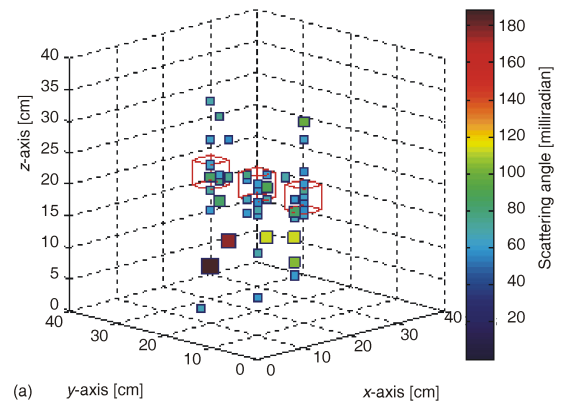
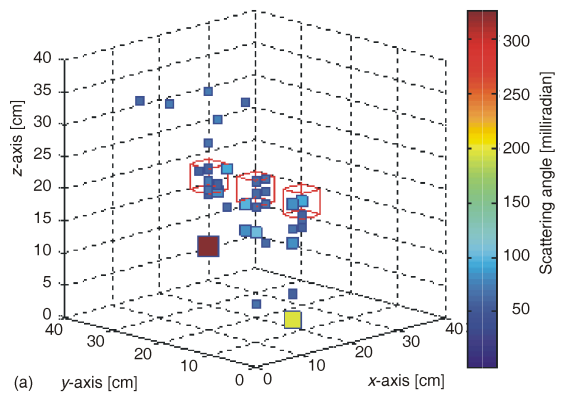


Figure 14. Refined cosmic muon tomography images of three tungsten cubes using (a) median filtering, (b) mean filtering, (c) mean filtering with Maxwell Boltzmann shift, and (d) integrated filtering algorithm

Figure 15. Refined cosmic muon tomography images of three uranium cubes using (a) median filtering, (b) mean filtering, (c) mean filtering with Maxwell Boltzmann shift, and (d) integrated filtering algorithm

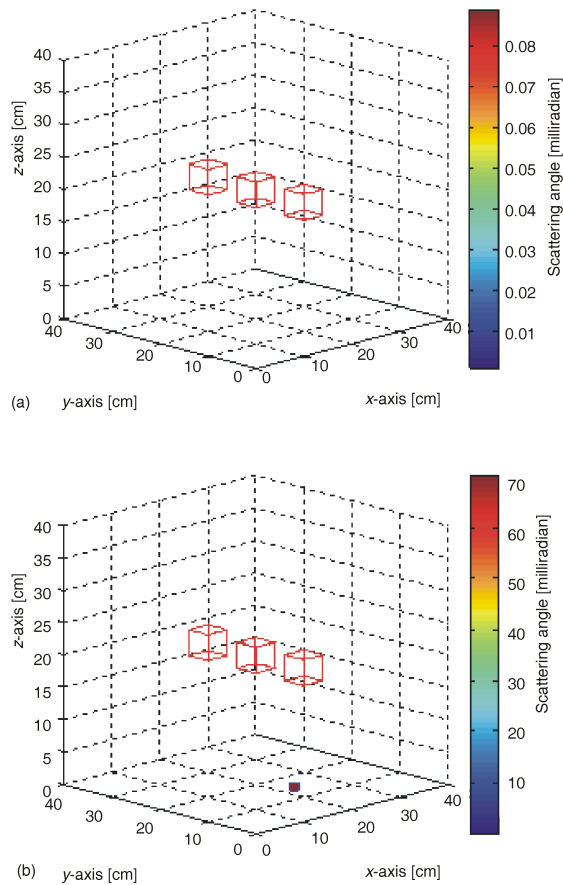


Figure 16. Refined cosmic muon tomography images; (a) three aluminum cubes and (b) three iron cubes using the integrated filter

indicators, a numerical analysis from the statistical hypothesis testing is adopted and the precision ratios are obtained based on:

Precision ratio = (Recognized in the correct position) / (Recognized in the correct position and the wrong position)

Precision ratio values for each of the analyzed statistical filtering methods are shown in tabs. 3, 4, and 5.

The integrated algorithm with the standard deviation, σ , equal to 1 in eq. (21), shows the best precision value; however only one scattering angle has a higher value than the threshold to detect three lead cubes as presented in tab. 3. This means that the other two lead cubes are not recognized as being made of high- Z material. Therefore, the standard deviation, σ , of 0.7, as defined in eq. (21), is selected as an adequate standard deviation for the filtering method. The average precision from the PoCA reconstruction is 13 %; from the integrated method, 88 %. This method results in a seven-fold improvement in precision analysis, on average.

Table 6 presents close to 97,700 scattering angle values obtained with the PoCA reconstruction method and 5,832 scattering angle values obtained with the integrated filtering algorithm. Fewer scattering angle

Table 3. Precision ratios of each statistical filtered tomography image for lead cubes

	Precision ratio	Precision ratio in [%]
PoCA	687/6381	11 %
Median filtering	6/18	33 %
Mean filtering	46/83	55 %
a*	39/71	55 %
b*($\sigma = 0.5$)	31/51	61 %
b*($\sigma = 0.7$)	16/17	94 %
b*($\sigma = 1$)	1/1	100 %
b*($\sigma = 1.5$)	0/0	–

a* mean filtering with Maxwell Boltzmann shift

b* integrated filtering algorithm

Table 4. Precision ratios of each statistical filtered tomography image for tungsten cubes

	Precision ratio	Precision ratio in [%]
PoCA	936/6567	14 %
Median filtering	24/46	52 %
Mean filtering	61/128	48 %
a*	58/111	52 %
b*($\sigma = 0.5$)	56/83	67 %
b*($\sigma = 0.7$)	49/56	88 %
b*($\sigma = 1$)	25/25	100 %
b*($\sigma = 1.5$)	0/0	–

Table 5. Precision ratios of each statistical filtered tomography image for uranium cubes

	Precision ratio	Precision ratio in [%]
PoCA	866/6458	13 %
Median filtering	19/36	53 %
Mean filtering	60/133	45 %
a*	57/113	50 %
b*($\sigma = 0.5$)	52/79	66 %
b*($\sigma = 0.7$)	43/52	83 %
b*($\sigma = 1$)	1/1	100 %
b*($\sigma = 1.5$)	0/0	–

Table 6. Comparison of the total number of scattering angles obtained with PoCA reconstruction method and integrated filtering algorithm

Material	Data from the PoCA reconstruction	Data from the integrated filtering algorithm
Lead	97668	5832
Tungsten	97694	5832
Uranium	97673	5832

values were obtained with the integrated filtering algorithm, demonstrating its ability to reduce the number of data points needed for analysis. The increase in precision, accompanied by the reduction of necessary data, allows for shorter inspection time; which is an important factor for cargo monitoring.

CONCLUSIONS

Cosmic muon tomography is an emerging technology employed to detect high-Z materials in cargo [48]. However, cosmic muons scatter off to non-uniformed scattering angles, producing noise in the tomography image. Hence, if cosmic muon tomography uses only the PoCA reconstruction method, its clarity and precision are limited.

To resolve this limitation, an integrated filtering algorithm, which is mainly composed of three statistical filtering methods, is introduced. The algorithm was tested to distinguish between high-Z, low-Z, and medium-Z materials. The integrated filtering algorithm shows seven times better improvement in the precision than the PoCA method. An additional advantage to the integrated filtering method is data reduction; this ultimately reduces the inspection time.

For future work, the application of muon tomography can also be extended to the real-time monitoring of nuclear facilities and inventories for the purpose of nuclear non-proliferation and reactor safety. However, in these applications, the random scattering angles between cosmic muons and nuclear fuels will produce noise in generated muon tomography images. Therefore, the developed integrated filtering method may be used to reduce noise and to increase detection precision.

ACKNOWLEDGEMENT

This research was supported jointly by the Utah Nuclear Engineering Program and the Ministry of National Defense of the Republic of Korea.

AUTHORS' CONTRIBUTIONS

S. Lee: modeled muon interactions using Geant4 and created the Point of Closest Approach module to reconstruct tomography image; developed the integrated filtering algorithm to refine muon tomography images; verified the algorithm showing improved tomography precision.

A. Foley: completed the linear correlation of eq. (20) between mean and mode values by fitting with Maxwell-Boltzmann distribution.

T. Jevremovic: Led the research and provided the review of the presented results.

REFERENCES

[1] Borozdin, K. N., et al., Surveillance: Radiographic Imaging with Cosmic-Ray Muons, *Nature*, 422 (2003), 6929, pp. 277-277
[2] Perry, J., Imaging a Nuclear Reactor Using Cosmic Ray Muons, *Journal of Applied Physics*, 113 (2013), 18, pp. 184909-184909-9
[3] Moliere, G. Z., Theory of the Scattering of Fast Charged Particles II, Multiple and Multiple Scattering, *Z. Naturforsch., Part A*, 3 (1948), p. 78

[4] Lynch, R.G., Orin, I. D., Approximations to Multiple Coulomb Scattering, *Nuclear Instruments & Methods in Physics Research, Section B, Beam Interactions with Materials and Atoms*, 58 (1991), 1, pp. 6-10
[5] Gaisser, T. K., Stanev, T., Cosmic Rays, *The European Physical Journal C – Particles and Fields*, 15 (2000), 1-4, pp. 150-156
[6] Morris, C. L., Tomographic Imaging with Cosmic Ray Muons, *Science & Global Security*, 16 (2008), 1, pp. 37-53
[7] Schultz, L. J., Statistical Reconstruction for Cosmic Ray Muon Tomography, *IEEE Transactions on Image Processing*, 16 (2007), 8, pp. 1985-1993
[8] Furlan, M., Application of Muon Tomography to Detect Radioactive Sources Hidden in Scrap Metal Containers, *IEEE Transactions on Nuclear Science*, 64 (2014), 4, pp. 2204-2209
[9] Mahan, G. D., Many-Particle Physics, Springer Science & Business Media, New York, USA, 2013
[10] Neddermeyer, S. H., Anderson, C. D., Note on the Nature of Cosmic-Ray Particles, *Physical Review*, 51 (1937), 10, pp. 884-886
[11] Hagiwara, K., et al., Review of Particle Properties, *Physical Review D*, 66 (2002), 1, 010001
[12] Helder, E., et al., Measuring the Cosmic-Ray Acceleration Efficiency of a Supernova Remnant, *Science*, 325 (2009), 5941, pp. 719-722
[13] Groom, D. E., Mokhov, N. V., Striganov, S. I., Muon Stopping Power and Range Tables 10 MeV-100 TeV, *Atomic Data and Nuclear Data Tables*, 78 (2001), 2, pp. 183-356
[14] Nakamura, K., Group, P. D., Review of Particle Physics, *Journal of Physics G: Nuclear and Particle Physics*, 37 (2010), 7A, 075021
[15] Hall, R., Lind, D., Ristinen, R., A simplified Muon Lifetime Experiment for the Instructional Laboratory, *Am. J. Phys.*, 38 (1970), 10, pp. 1196-1200
[16] Lange, S., Aulich, A., Lanksch, W., Image Artefacts in Computerized Tomography, in: *Cranial Computerized Tomography* (Eds. W. Lanksch E. Kazner), 1976, Springer, Berlin, Heidelberg, pp. 69-72
[17] Cherry, S. R., Multimodality Imaging: Beyond pet/ct and spect/ct. in *Seminars in Nuclear Medicine*, *WB Saunders*, 39 (2009), 5, pp. 348-353
[18] Marteau, J., et al., Muons Tomography Applied to Geosciences and Volcanology, *Nuclear Instruments and Methods in Physics Research Section A: Accelerators, Spectrometers, Detectors and Associated Equipment*, 695 (2012), pp. 23-28
[19] Durham, J. M., Imaging the Core of Fukushima Reactor with Muons, No. LA-UR-15-24802, LANL, NM, USA 2015
[20] Sunday, D., Distance Between Lines and Segments with Their Closest Point of Approach, URL: <http://www.softsurfer.com/Archive/algorithm, 2004>
[21] Lohmann, W., Kopp, R., Voss, R., Energy Loss of Muons in the Energy Range 1-10000 GeV, *CERN*, 85 (1985), 3, pp. 1-9
[22] Hohlmann, M., et al., GEANT4 Simulation of a Cosmic Ray Muon Tomography System with Micro-Pattern Gas Detectors for the Detection of High-Materials, *Nuclear Science, IEEE Transactions on*, 56 (2009), 3, pp. 1356-1363
[23] Bethe, H., Theory of Passage of Swift Corpuscular Rays Through Matter, *Ann. Physik*, 5 (1930), p. 325
[24] Bogdanov, A. G., et al., Geant-4 Simulation of High Energy Muon Interactions, in: *Nuclear Science Symposium Conference Record*, IEEE, 2004, pp. 2043-2047
[25] Knoll, G. F., *Radiation Detection and Measurement*, John Wiley & Sons, New York, USA, 2010

- [26] Davies, H., Bethe, H., Maximon, L., Theory of Bremsstrahlung and Pair Production, II. Integral Cross Section for Pair Production, *Physical Review*, 93 (1954), 4, pp. 788-795
- [27] Rozental', I., Interaction of Cosmic Muons of High Energy, *Physica-Usppekhi*, 11 (1968), 1, pp. 49-65
- [28] Kelner, S., Kotov, Y. D., Muon Energy Loss to Pair Production, *Soviet Journal of Nuclear Physics*, 7 (1968), 2, pp. 237-&
- [29] Voss, R., Deep-Inelastic Scattering with Muons, *Physics Reports*, 403 (2004), 1, pp. 3-18
- [30] Halzen, F., Martin, A. D., *Quark & Leptons: An Introductory Course in Modern Particle Physics*, John Wiley & Sons, New York, USA, 2008
- [31] Bethe, H. A., Moliere's Theory of Multiple Scattering, *Physical Review*, 89 (1953), 6, pp. 1256-1266
- [32] Pentia, M., Iorgovan, G., Mihul, A., Multiple Scattering Error Propagation in Particle Track Reconstruction, *Romanian Journal of Physics*, 40 (1994), pp. 181-191
- [33] Carlisle, T., Cobb, J., Neuffer, D., Multiple Scattering Measurements in the MICE Experiment, 2013
- [34] Tsai, Y.-S., Pair Production and Bremsstrahlung of Charged Leptons, *Reviews of Modern Physics*, 46 (1974), 4, pp. 815-952
- [35] Gustafsson, J., Tomography of Canisters for Spent Nuclear Fuel Using Cosmic-Ray Muons, Uppsala University, INF, UU-NF05, 2005, 8
- [36] Schultz, L. J., et al., Image Reconstruction and Material Z Discrimination via Cosmic Ray Muon Radiography, *Nuclear Instruments and Methods in Physics Research Section A: Accelerators, Spectrometers, Detectors and Associated Equipment*, 519 (2004), 3, pp. 687-694
- [37] Hoch, R., et al., Muon Tomography Algorithms for Nuclear Threat Detection, in: *Opportunities and Challenges for Next-Generation Applied Intelligence*, Springer, 2009, pp. 225-231
- [38] Gnanvo, K., et al., Imaging of High-Z Material for Nuclear Contraband Detection with a Minimal Prototype of a Muon Tomography Station Based on GEM Detectors, *Nuclear Instruments and Methods in Physics Research, Section A: Accelerators, Spectrometers, Detectors and Associated Equipment*, 652 (2011), 1, pp. 16-20
- [39] Agostinelli, S., et al., GEANT4-a Simulation Toolkit, *Nuclear Instruments and Methods, in: Physics Research Section A: Accelerators, Spectrometers, Detectors and Associated Equipment*, 506 (2003), 3, pp. 250-303
- [40] Clarkson, A., et al., GEANT4 Simulation of a Scintillating-Fibre Tracker for the Cosmic-Ray Muon Tomography of Legacy Nuclear Waste Containers, *Nuclear Instruments and Methods in Physics Research Section A: Accelerators, Spectrometers, Detectors and Associated Equipment*, 746 (2014), pp. 64-73
- [41] Borozdin, K., et al., Cosmic-Ray Muon Tomography and its Application to the Detection of High-Z Materials, *Proceedings*, 46th Annual Meeting, Institute of Nuclear Materials Management, Phoenix, Ariz., USA, 2005
- [42] Shapiro, L.G., Stockman, G. C., *Computer Vision*, Prentice Hall, 2001
- [43] Huang, T. S., A Fast Two-Dimensional Median Filtering Algorithm, *IEEE Transactions on Acoustics, Speech and Signal Processing*, 27 (1979), 1, pp. 13-18
- [44] Agarwal, B. L., *Basic Statistics*, New Age International Publisher, New Delhi, 2006
- [45] Papoulis, A., Pillai, S. U., *Probability, Random Variables, and Stochastic Processes*, Tata McGraw-Hill Education, New York, USA, 2002
- [46] Reichl, L.E., Prigogine, I., *A Modern Course in Statistical Physics*, Vol. 71, University of Texas press Austin, Tex., USA, 1980
- [47] Haddad, R. A., A Class of fast Gaussian Binomial Filters for Speech and Image Processing, *IEEE Transactions on Signal Processing*, 39 (1991), 3, pp. 723-727
- [48] Gnanvo, K., Imaging of High-Z Material for Nuclear Contraband Detection with a Minimal Prototype of a Muon Tomography Station Based on GEM Detectors, *Nuclear instruments & Methods in Physics Research, Section A, Accelerators, Spectrometers, Detectors and Associated Equipment*, 652 (2011), 1, pp. 16-20

Received on February 4, 2016

Accepted on March 7, 2016

Санкју ЛИ, Аманда ФОЛЕЈ, Татјана ЈЕВРЕМОВИЋ

НОВИ АЛГОРИТАМ ЗА ПРЕЦИЗНУ И ЕФИКАСНУ АНАЛИЗУ МИОНСКЕ ТОМОГРАФИЈЕ

У овом раду приказујемо нови алгоритам са повећаном прецизношћу и ефикасношћу мионске томографије, са применама у детекцији нуклеарних материјала. Космичка мионска томографија је техника испитивања која се последњих деценија све више користи за детекцију тешких материјала присутних у одређеној запремини. Техника мионске томографије заснива се на угловима расејања миона на основу којих се заправо генерише слика испитиване геометрије. Углови расејања миона после интеракција нису униформни зато што миони имају спектар енергија. Неуниформна расподела углова расејања миона повећава нејасноћу приказане слике. GEANT4 је коришћен да се нумеричким путем генеришу подаци о мионском расејању (углови и позиције) у геометрији унапред дефинисаној, са садржајем материјала високог Z. Генерисани имици су онда процесирани методом "closest approach" (PoCA); статистички филтеринг метод је затим развијен са циљем да се реконструише PoCA слика. Тако испроцесуирана слика показује повећану јасноћу, прецизину је у одређивању присутности разних материјала, што овај метод чини ефикаснијим у поређењу са PoCA методом. Повећана прецизност достиже 88 % у поређењу са PoCA прецизношћу од само 13 % у детекцији нуклеарних и других тешких материјала.

Кључне речи: мионска томографија, вишесироко кулоновско расејање, GEANT-4, нуклеарни материјал